

## Mesoscopic Free Path of Nonthermalized Photogenerated Carriers in a Ferroelectric Insulator

Zongquan Gu and Dominic Imbrenda

*Department of Electrical and Computer Engineering, Drexel University, Philadelphia, Pennsylvania 19104, USA*

Andrew L. Bennett-Jackson, Matthias Falmbigl, and Adrian Podpirka

*Department of Materials Science and Engineering, Drexel University, Philadelphia, Pennsylvania 19104, USA*

Thomas C. Parker, Daniel Shreiber, and Mathew P. Ivill

*U.S. Army Research Laboratory, Aberdeen Proving Ground, Maryland 21005, USA*

Vladimir M. Fridkin\*

*Shubnikov Institute of Crystallography, Russian Academy of Sciences,  
Leninsky Prospect 59, Moscow 117333, Russian Federation*

Jonathan E. Spanier†

*Department of Materials Science and Engineering, Drexel University, Philadelphia, Pennsylvania 19104, USA*

(Received 18 October 2016; published 1 March 2017)

We show how finite-size scaling of a bulk photovoltaic effect-generated electric field in epitaxial ferroelectric insulating BaTiO<sub>3</sub>(001) films and a photo-Hall response involving the bulk photovoltaic current reveal a large room-temperature mean free path of photogenerated nonthermalized electrons. Experimental determination of mesoscopic ballistic optically generated carrier transport opens a new paradigm for hot electron-based solar energy conversion, and for facile control of ballistic transport distinct from existing low-dimensional semiconductor interfaces, surfaces, layers, or other structures.

DOI: [10.1103/PhysRevLett.118.096601](https://doi.org/10.1103/PhysRevLett.118.096601)

Ballistic transport of carriers is a celebrated feature of selected two- and one-dimensional systems [1–6] in which the mean free path is limited by scattering by other carriers, defects, and phonons. In band insulators, however, such transport is impossible within the material bulk, even in crystals of exceptional quality. The bulk photovoltaic effect (BPE) in crystals without a center of symmetry [7–11] is caused by asymmetric distribution of nonthermalized carrier momentum, a consequence of the violation of the Boltzmann principle of detailed balance [10], and is analogous to parity nonconservation in the weak interaction [12]. Long after the discoveries of remarkably large photovoltages in SbSI [7] and LiNbO<sub>3</sub> [8], photovoltaic effects in ferroelectrics have attracted renewed attention [11,13–23]. While photovoltages in ferroelectrics can greatly exceed the band gap, the direct conversion of light energy to electricity has been extremely low until recently [14,22,23]. Carrier separation and photogenerated current collection in ferroelectrics can arise in principle from several effects, including spatial variation in electrostatic potential due to interfaces or interfacial regions, e.g., domain walls and/or space charge at and near the ferroelectric-metal interface, transient responses due to pyroelectric and depolarizing field effects, and effects caused by inhomogeneous illumination. In conventional solar cells the collection of photogenerated carriers is bounded by their diffusion

length. In the bulk photovoltaic effect (BPE), however, knowledge of the free path of hot electrons in such states is paramount to understanding and improving conversion efficiency.

The BPE involving spatially homogenous illumination in crystals lacking center of inversion symmetry exists even in the absence of these aforementioned effects. The BPE and the resulting separation of photogenerated electrons and holes have been explained by two possible mechanisms: ballistic and shift. The ballistic mechanism is associated with the excitation of nonthermalized (hot) carriers in a noncentrosymmetric crystal, leading to an asymmetric distribution of nonthermalized carrier momentum and a violation of the Boltzmann principle of detailed balance [10]. In the ballistic mechanism the photoexcited nonthermalized carriers lose their energy and descend to the bottom of the conduction band over a free path, i.e., thermalization length  $l_0$ . Shift current, the alternative mechanism for the BPE, is obtained by accounting for the nondiagonal elements of the density matrix [9,24], established within the framework of density functional theory [11,25]. One interpretation of this shift mechanism shows that, in spite of the coexistence of the two mechanisms, shift current evolution does not involve inertia [10]. On the contrary, the ballistic current is caused by free carrier transport and contributes to the (photo-)Hall

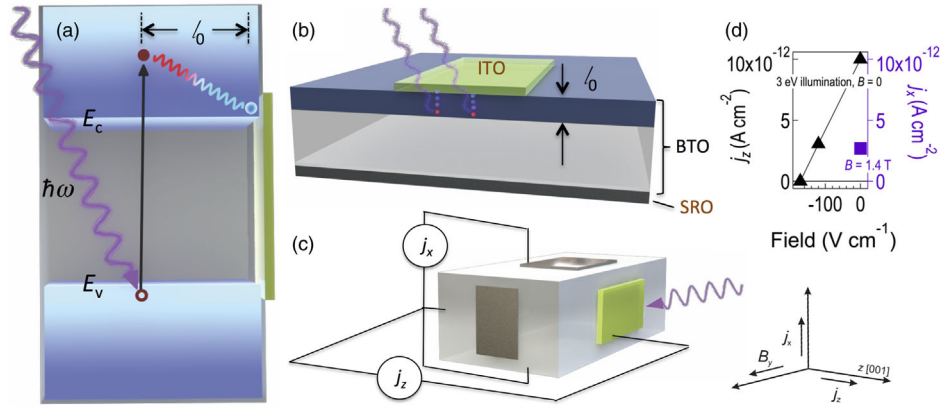


FIG. 1. (a) Schematic band diagram illustrating the photoexcitation process in a noncentrosymmetric crystal depicting cooling of hot photogenerated bulk photovoltaic effect carriers collected only within a thermalization length  $l_0$ . Illustration of experimental geometry of (b) epitaxial BaTiO<sub>3</sub> (BTO) (001) film on a SrRuO<sub>3</sub> (SRO) bottom electrode used to determine thermalization length  $l_0$ , (c) photo-Hall measurements carried out on a bulk single crystal under 3 eV illumination exhibiting ballistic conduction in the ferroelectric insulator BaTiO<sub>3</sub> crystal at 300 K, and (d) current and photo-Hall current densities under zero and  $B = 1.4$  T field.

effect. Nevertheless, both mechanisms can contribute to the BPE.

In the bulk crystal the power conversion efficiency via the BPE is extremely small, i.e.,  $10^{-5}$ – $10^{-6}$ . It was shown that in nanoscale-thickness BaTiO<sub>3</sub> films, the internal power conversion efficiency (under monochromatic illumination,  $\lambda = 360$  nm) is enhanced by more than 4 orders of magnitude, to  $\lesssim 1\%$  [23]. This finite-size effect can be explained phenomenologically in terms of the ballistic mechanism.

The tensor properties of the linear BPE current are described [10] by

$$J_i = G_{ijl}^L e_j e_l^* I + iG_{il}^C [ee^*]_i I, \quad (1)$$

where  $e_j$  and  $e_l$  are components of the light polarization vector,  $G_{ijl}^L$  is the corresponding third-rank tensor (for point group  $C_{4v}$  of BaTiO<sub>3</sub>), and  $I$  is the incident light intensity. ( $G_{il}^C$  is a second-rank tensor relevant for gyrotropic materials.) For unpolarized radiation, the first term of Eq. (1) can be written in its scalar form,  $j_{pv} = G_{31} I = \alpha g_{31} I$ , where  $\alpha$  is the BaTiO<sub>3</sub> film absorption coefficient (for  $\hbar\omega \approx 3$  eV  $\alpha \approx 150$  cm<sup>-1</sup>).

The field  $E_{pv}$  generated by the current  $j$  is given by  $E_{pv} = j/\sigma_{ph}$ , where  $\sigma_{ph} = e\varphi\alpha l(\hbar\omega)^{-1}(\mu\tau)$  is the photoconductivity. Here,  $e$  is the elementary charge,  $\varphi \leq 1$  is the quantum yield,  $\hbar\omega$  is the quantum of energy, and  $\mu$  and  $\tau$  are the mobility and lifetime of nonequilibrium carriers, respectively. Thus, the field generated by the BPE current is

$$E_{pv} = \frac{g_{31}\hbar\omega}{e\varphi(\mu\tau)}. \quad (2)$$

It is seen from Eq. (2) that the finite-size effect on  $E_{pv}$  and on the internal power conversion efficiency ( $=g_{31}E_{pv}/4$ ) [10,23] is caused by the thermalization. Following thermalization the hot electrons become

(thermalized) polarons, which do not contribute to the BPE due to their symmetric momentum distribution. The finite-size effect is related to  $(\mu\tau)_{nt} \ll (\mu\tau)_t$ , where  $(\mu\tau)_{nt}$  and  $(\mu\tau)_t$  are the mobility-lifetime products for nonthermalized and thermalized electrons, respectively, and, correspondingly,  $E_{pv}^t \ll E_{pv}^{nt}$ . Simultaneously, internal power conversion efficiency strongly decreases for  $l \gg l_0$ .

The ballistic theory of BPE for excitation from donors within a dipole-impurity model yields for the ballistic current [10,24]  $j^{\text{bal}} = e\varphi\alpha l(\hbar\omega)^{-1}l_0\xi$ , where  $l_0$  is the free path of nonthermalized electrons [Fig. 1(a)] and  $\xi = \xi(\hbar\omega)$  is a microscopic parameter that characterizes the asymmetry of the photoexcited electron momentum distribution. A dipole-impurity model for  $k_0a \approx 1$  suggests that  $\xi$  will not exceed  $\xi_{\text{max}} = 0.1$  [10,24], where  $k_0$  is momentum and  $a$  is the lattice constant (for BaTiO<sub>3</sub>,  $a \approx 0.4$  nm).

The ballistic nature of photogenerated electrons in ferroelectric BaTiO<sub>3</sub> is confirmed by a Hall mobility measurement of nonthermalized electrons in a single crystal [Figs. 1(c) and 1(d)] under illumination along [001] at 300 K. Photovoltaic current density  $j_z$  was collected along [001] at several values of applied electric field  $E$  and no magnetic field ( $B = 0$ ) using semitransparent electrodes, yielding  $g_{31} = 2 \times 10^{-8}$  cm/V, in agreement with earlier work [23], with short-circuit current density  $j_{z0} = 1.0 \times 10^{-11}$  A/cm<sup>2</sup>. Application of the magnetic field  $B = 1.4$  T along [010] produced a Hall component  $j_x = 2.7 \times 10^{-12}$  A/cm<sup>2</sup>. The mobility of nonthermalized electrons in the BPE regime [10] is  $\mu_{nt} = (1/B)(j_x/j_z) \approx 1900$  cm<sup>2</sup> V<sup>-1</sup> s<sup>-1</sup> [14], 3 orders of magnitude larger than that for thermalized carriers, demonstrating that the BPE in BaTiO<sub>3</sub> under 3 eV illumination is caused by ballistic transport [26]. Significantly, this room-temperature value for  $\mu_{nt}$  is also 1–2 orders of magnitude higher than the highest room-temperature carrier mobility reported for any complex oxide interface [4], surface [27], or bulk [28]. This

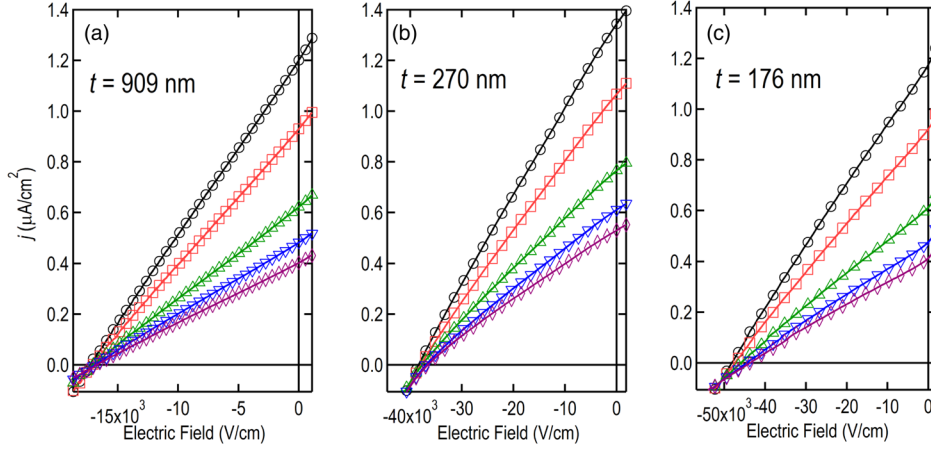


FIG. 2. Representative bulk photovoltaic responses in epitaxial  $\text{BaTiO}_3(001)$  films of thickness denoted in each panel. Films were deposited on  $\text{SrRuO}_3$  film bottom electrodes on  $\text{SrTiO}_3(100)$  and responses measured under a range of intensities. The intensities in (a) and (b) are 0.182 (black circles), 0.145 (red squares), 0.101 (green triangles), 0.078 (blue triangles), and 0.067 (magenta diamonds)  $\text{W}/\text{cm}^2$ , and the intensities in (c) are 0.142 (black circles), 0.113 (red squares), 0.076 (green triangles), 0.060 (blue triangles), and 0.051 (magenta diamonds)  $\text{W}/\text{cm}^2$  of monochromatic 3.06 eV (405 nm) illumination.

permits us to get a rough estimate of  $l_0$  for  $\text{BaTiO}_3$ . From the above,  $g_{31} = e\varphi(\hbar\omega)^{-1}l_0\xi$ . The values of the tensor component  $G_{31}(= \alpha g_{31})$  are known for many ferro- and piezoelectrics [10]. Substituting for  $\text{BaTiO}_3$   $g_{31} \approx 10^{-8} \text{ cm V}^{-1}$  and  $\hbar\omega = 3 \text{ eV}$ , one obtains  $l_0 \approx 0.1(\varphi\xi)^{-1} \approx 10 - 100 \text{ nm}$ .

Another estimate of  $l_0$  can be obtained from the non-thermalized photo-Hall mobility of the ballistic electrons,

$$\mu_{\text{nt}} \approx \frac{e}{m^*} \tau_{\text{nt}} \approx \frac{el_0}{\hbar k_0}, \quad (3)$$

where  $k_0 a \approx 1$ . For  $\mu_{\text{nt}} \approx 1.9 \times 10^3 \text{ cm}^2 \text{ V}^{-1} \text{ sec}^{-1}$  and  $a \approx 0.4 \text{ nm}$ ,

$$l_0 \approx \frac{\hbar}{ea} \mu_{\text{nt}} \approx 40 \text{ nm}. \quad (4)$$

We next describe the finite-size evolution of the BPE in single-domain  $\text{BaTiO}_3(001)$  epitaxial films ranging in thickness as  $8 \lesssim l \lesssim 900 \text{ nm}$ , synthesized by pulsed laser deposition on  $\text{SrRuO}_3/\text{SrTiO}_3(100)$  (see Supplemental Material [29]). Using  $\text{SrRuO}_3$  and lithographically patterned indium tin oxide (ITO) films as planar bottom and top electrodes, respectively [Fig. 1(b)],  $\text{BaTiO}_3$  films exhibited ferroelectric hysteresis (see Supplemental Material [29]) and were subsequently electrically poled along [001] with the  $\text{SrRuO}_3$  bottom electrode held at a positive voltage with respect to the grounded ITO top electrode (i.e., polarization oriented upward). In accordance with tensor  $G$  at illumination along [001] for our geometry,  $E_{\text{pv}}$  is directed antiparallel to the direction of spontaneous polarization  $P$ , and the photovoltaic current flows in the same direction, [001]. Dependences of photovoltaic current on bias voltage were collected in each thin film under unpolarized monochromatic 3.06 eV illumination for a

range of different incident intensities up to  $\approx 0.18 \text{ W}/\text{cm}^2$ , examples of which are shown in Fig. 2. The short-circuit current  $j_{\text{sc}}$  is linear with intensity (Fig. 3), yielding  $g_{31} \approx 10^{-8} \text{ cm V}^{-1}$ .

From the linear current density-voltage characteristic  $j = j(V)$ , thickness-dependent values of the photovoltaic field  $E_{\text{pv}}(l)(=V/l)$  were obtained, showing a finite-size effect of  $E_{\text{pv}} = E_{\text{pv}}(l)$  [Fig. 4(a)].  $E_{\text{pv}}$  increases from  $\approx 170 \text{ V cm}^{-1}$  in the 0.4-cm-thick crystal, which corresponds to the bulk value [10], approaching  $10^5 \text{ V cm}^{-1}$  for the 8-, 14-, 42-, and 88-nm-thick films. Concomitantly, the

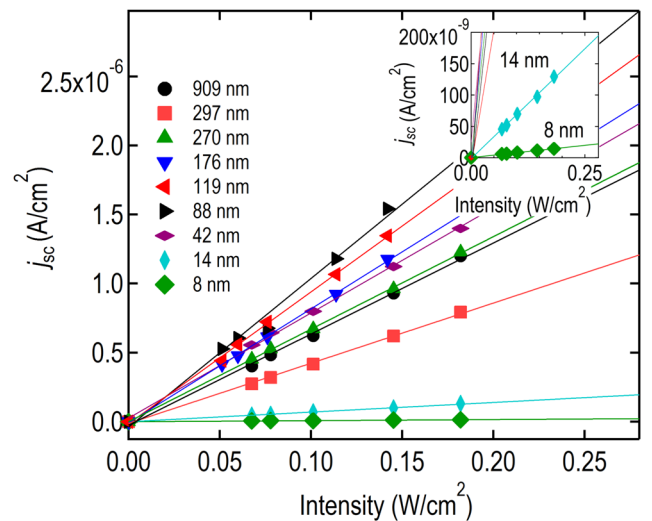


FIG. 3. Linear dependence of short-circuit current  $j_{\text{sc}}$  on incident light intensity enabling determination of values of photovoltaic tensor component  $g_{31}$ . Plotted in the inset is an expanded range of current, showing data for the two thinnest films.

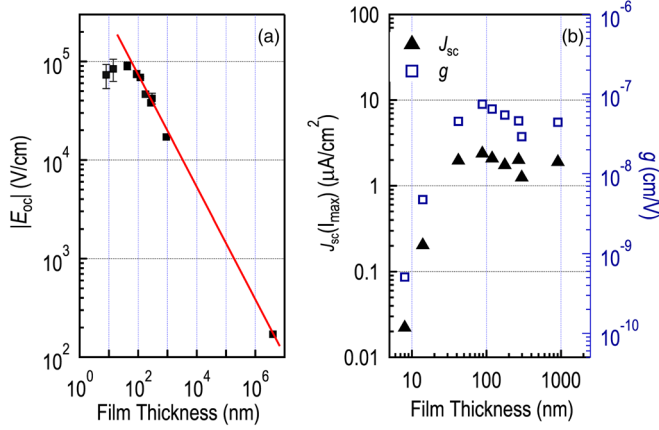


FIG. 4. (a) Finite-thickness scaling of the magnitude of photo-voltaic field  $|E_{oc}(l)|$  in epitaxial single-domain  $\text{BaTiO}_3(001)$  films and a macroscopic  $\text{BaTiO}_3$  crystal revealing onset of saturation for  $l \approx 100$  nm and identification of scale of mean free path  $l_0$  for  $\hbar\omega \approx 3.1$  eV. The line is added as a guide to the eye, intersecting data points in a range over which the variation is clearly linear. (b) Short-circuit current density  $j_{sc}$  and photovoltaic scalar  $g$  with thickness revealing a sharp decrease for thinner films.

internal power conversion efficiency increases by 3 orders of magnitude. It is seen from Fig. 4(a) that for  $l \lesssim 100$  nm,  $E_{pv} \lesssim 10^5$  V cm $^{-1}$ , i.e., less than the Landau-Ginzburg intrinsic coercive field for  $\text{BaTiO}_3$  ( $\approx 10^8$  V cm $^{-1}$ ), accounting for the absence of switching in the nanoscale films by the BPE field. From the saturation value  $E_{pv} \approx 10^5$  V cm $^{-1}$  and the above calculations, one can evaluate the lifetime of nonthermalized electrons  $\tau_{nt}$ . Substituting  $g_{31} \approx 10^{-8}$  cm V $^{-1}$ ,  $\mu_{nt} \approx 10^3$  cm $^2$  V $^{-1}$  sec $^{-1}$ , and  $\hbar\omega \approx 3$  eV gives  $\tau_{nt} \approx 3 \times 10^{-13} \varphi^{-1}$  sec, which is in reasonable agreement with the typical relaxation time of nearly free electrons:  $\tau_{nt} = \mu_{nt} m / e \approx 10^{-12} - 10^{-14}$  sec [32].

Interestingly,  $j_{sc}$  and  $g$  for the thinnest films drop 2 orders of magnitude within a single decade of thickness reduction [Fig. 4(b)]. Simultaneously,  $E_{oc}$  remains essentially unchanged. Band bending in the thinnest films is likely present and is caused by the screening of spontaneous polarization. It is determined by the Debye screening length, which is on the order of  $L_D \approx 10$  nm for insulating  $\text{BaTiO}_3$  with a low concentration of carriers [33]. This bending at the surface leads to a decrease of  $g$  (or of  $j_{sc}$ ), as seen in Fig. 4(b). But the generated field  $E_{oc} = E_{pv} \approx (j_{sc} / \sigma_{ph})$  remains essentially unchanged because the photo-conductivity  $\sigma_{ph}$  is also decreased due to the volume screening charge and possible decrease of the lifetime. Our observation is presently limited by two experimental points in this thickness range, and it does not permit us to claim this conclusively. Nevertheless, the data in Fig. 4(a) indicate good agreement with the theoretically predicted value of the nonthermalized electron free path  $l_0 \approx 100$  nm for 3 eV excitation. Clearly, for the shift current the induced field  $E_{pv}$  must also reveal the finite-size effect caused by

thermalization of electrons which are responsible for photoconductivity. But the shift current itself does not involve carrier transport, and for films with thicknesses comparable with the shift vector magnitude [11], the finite-size effect can be different.

In conclusion, we have shown how the free path of photogenerated nonthermalized electrons can be determined experimentally, remarkably yielding a mesoscopic value that is in good agreement with theoretically predicted values, for 3 eV. The nonequilibrium carriers, which are responsible for the ballistic photovoltaic current, have extremely high mobility. A new strategy for efficient photovoltaic solar energy conversion relies on hot carriers photogenerated within and collected from colocating volumes of thermalization and screening in nanoscale electrode-interfaced ferroelectrics [13,14]. An experimental prescription revealing an unexpectedly long room-temperature mean free path of photogenerated carriers in a ferroelectric insulator is key to advancing the promise of efficient bulk photovoltaic effect-based solar energy conversion.

This work was supported by the U.S. Army Research Office under Grant No. W911NF-14-1-0500. Z. G. was supported by the National Science Foundation and the Semiconductor Research Corporation under the Nanoelectronics in 2020 and Beyond Program under Grant No. DMR 1124696. M. F. was supported by the Office of Naval Research under Grant No. N00014-1501102170. A. P. was supported by the SunShot Program of the U.S. Department of Energy under Grant No. DE-SC0014664. The research was partially sponsored by the Army Research Laboratory and was accomplished under Cooperative Agreement No. W911NF-12-2-0019. The authors acknowledge the Drexel core shared facilities and NSF DMR 1040166.

Z. G. and D. I. contributed equally to this work.

\*Also at Department of Physics, Drexel University, Philadelphia, PA 19104, USA.

†Also at Department of Physics, and Department of Electrical and Computer Engineering, Drexel University, Philadelphia, PA 19104, USA.  
spanier@drexel.edu

- [1] T. Ando, A. B. Fowler, and F. Stern, *Rev. Mod. Phys.* **54**, 437 (1982).
- [2] M. Bockrath, D. H. Cobden, P. L. McEuen, N. G. Chopra, A. Zettl, A. Thess, and R. E. Smalley, *Science* **275**, 1922 (1997).
- [3] S. J. Tans, M. H. Devoret, H. Dai, A. Thess, R. E. Smalley, L. J. Geerligs, and C. Dekker, *Nature (London)* **386**, 474 (1997).
- [4] A. Ohtomo and H. Y. Hwang, *Nature (London)* **427**, 423 (2004).
- [5] K. S. Novoselov, A. K. Geim, S. V. Morozov, D. Jiang, M. I. Katsnelson, I. V. Grigorieva, S. V. Dubonos, and A. A. Firsov, *Nature (London)* **438**, 197 (2005).



- [6] Y. Zhang, Y. W. Tan, H. L. Stormer, and P. Kim, *Nature (London)* **438**, 201 (2005).
- [7] A. A. Grekov, M. A. Malitskaya, V. D. Spitsina, and V. M. Fridkin, *Kristallografiya* **15**, 500 (1970) [*Sov. Phys. Crystallogr.* **15**, 423 (1970)].
- [8] A. M. Glass, D. von der Linde, and T. J. Negran, *Appl. Phys. Lett.* **25**, 233 (1974).
- [9] R. von Baltz and W. Kraut, *Phys. Rev. B* **23**, 5590 (1981).
- [10] B. Sturman and V. Fridkin, *The Photovoltaic and Photorefractive Effects in Noncentrosymmetric Materials* (Gordon and Breach, Philadelphia, 1992).
- [11] S. M. Young and A. M. Rappe, *Phys. Rev. Lett.* **109**, 116601 (2012).
- [12] C. S. Wu, E. Ambler, R. W. Hayward, D. D. Hoppes, and R. P. Hudson, *Phys. Rev.* **105**, 1413 (1957).
- [13] M. Alexe and D. Hesse, *Nat. Commun.* **2**, 256 (2011).
- [14] J. E. Spanier, V. M. Fridkin, A. M. Rappe, A. R. Akbashev, A. Polemi, Z. Gu, Y. Qi, S. M. Young, D. Imbrenda, G. Xia *et al.*, *Nat. Photonics* **10**, 611 (2016).
- [15] S. Y. Yang, J. Seidel, S. J. Byrnes, P. Shafer, C. H. Yang, M. D. Rossell, P. Yu, Y. H. Chu, J. F. Scott, J. W. Ager *et al.*, *Nat. Nanotechnol.* **5**, 143 (2010).
- [16] J. Seidel, D. Fu, S.-Y. Yang, E. Alarcón-Lladó, J. Wu, R. Ramesh, and J. W. Ager, *Phys. Rev. Lett.* **107**, 126805 (2011).
- [17] J. Kreisel, M. Alexe, and P. A. Thomas, *Nat. Mater.* **11**, 260 (2012).
- [18] D. Daranciang, M. J. Highland, H. Wen, S. M. Young, N. C. Brandt, H. Y. Hwang, M. Vattilana, M. Nicoul, F. Quirin, J. Goodfellow *et al.*, *Phys. Rev. Lett.* **108**, 087601 (2012).
- [19] I. Grinberg, D. V. West, M. Torres, G. Gou, D. M. Stein, L. Wu, G. Chen, E. M. Gallo, A. R. Akbashev, P. K. Davies *et al.*, *Nature (London)* **503**, 509 (2013).
- [20] V. Fridkin, *IEEE Trans. Ultrason. Ferroelectr. Freq. Control* **60**, 1551 (2013).
- [21] A. Bhatnagar, A. Roy Chaudhuri, Y. Heon Kim, D. Hesse, and M. Alexe, *Nat. Commun.* **4**, 2835 (2013).
- [22] R. Nechache, C. Harnagea, S. Li, L. Cardenas, W. Huang, J. Chakrabarty, and F. Rosei, *Nat. Photonics* **9**, 61 (2015).
- [23] A. Zenkevich, Y. Matveyev, K. Maksimova, R. Gaynutdinov, A. Tolstikhina, and V. Fridkin, *Phys. Rev. B* **90**, 161409 (2014).
- [24] V. Belinicher and B. Sturman, *Sov. Phys. Usp.* **23**, 199 (1980).
- [25] S. M. Young, F. Zheng, and A. M. Rappe, *Phys. Rev. Lett.* **109**, 236601 (2012).
- [26] S. Astafiev, V. Fridkin, V. Lazarev, and A. Shlensky, *Ferroelectrics* **83**, 3 (1988).
- [27] J. Son, P. Moetakef, B. Jalan, B. O., N. J. Wright, R. Engel-Herbert, and S. Stemmer, *Nat. Mater.* **9**, 482 (2010).
- [28] S. Raghavan, T. Schumann, H. Kim, J. Y. Zhang, T. A. Cain, and S. Stemmer, *APL Mater.* **4**, 016106 (2016).
- [29] See Supplemental Material <http://link.aps.org/supplemental/10.1103/PhysRevLett.118.096601>, which includes Refs. [30, 31], for methods, x-ray diffraction, x-ray reflectivity, Rutherford backscattering spectroscopy, ferroelectric hysteresis, and film roughness data.
- [30] M. Björck and G. Andersson, *J. Appl. Crystallogr.* **40**, 1174 (2007).
- [31] B. Jaffe, *Piezoelectric Ceramics* (Academic Press, New York, 1978), Vol. 3.
- [32] C. Kittel, *Introduction to Solid State Physics* (John Wiley & Sons., New York, 1956).
- [33] V. Fridkin, *Ferroelectric Semiconductors* (Consultants Bureau, New York, 1980).